Title

Bright Infrared-to-Ultraviolet/Visible Upconversion in Small Alkaline Earth-Based Nanoparticles with Biocompatible CaF2 Shells

Journal

Angewandte Chemie International Edition, 59(48)

ISSN

1433-7851

Authors

Fischer, Stefan
Siefe, Chris
Swearer, Dayne F
et al.

Publication Date

2020-11-23

DOI

10.1002/anie.202007683

Peer reviewed

HHS Public Access

Author manuscript

Angew Chem Int Ed Engl. Author manuscript; available in PMC 2021 July 15.

Published in final edited form as:

Angew Chem Int Ed Engl. 2020 November 23; 59(48): 21603–21612. doi:10.1002/anie.202007683.

Bright Infrared-to-Ultraviolet/Visible Upconversion in Small Alkaline Earth-Based Nanoparticles with Biocompatible CaF_2 Shells

Stefan Fischer[+],
Department of Materials Science and Engineering, Stanford University, 496 Lomita Mall, Stanford, CA 94305 (USA)

Siefe Chris[+,*],
Department of Materials Science and Engineering, Stanford University, 496 Lomita Mall, Stanford, CA 94305 (USA)

Dayne F. Swearer,
Department of Materials Science and Engineering, Stanford University, 496 Lomita Mall, Stanford, CA 94305 (USA)

Claire A. McLellan,
Department of Materials Science and Engineering, Stanford University, 496 Lomita Mall, Stanford, CA 94305 (USA)

A. Paul Alivisatos,
Materials Science Division, Lawrence Berkeley National Laboratory, Berkeley, CA 94720 (USA), and Department of Chemistry, University of California, Berkeley, Berkeley, CA 94720 (USA), and Department of Materials Science and Engineering, University of California, Berkeley, Berkeley, CA 94720 (USA), and Kavli Energy Nanoscience Institute, Berkeley, CA 94720 (USA)

Jennifer A. Dionne[*]
Department of Materials Science and Engineering, Stanford University, 496 Lomita Mall, Stanford, CA 94305 (USA)

Abstract

Upconverting nanoparticles (UCNPs) are promising candidates for photon-driven reactions, including light-triggered drug delivery, photodynamic therapy, and photocatalysis. Herein, we investigate the NIR-to-UV/visible emission of sub-15 nm alkaline-earth rare-earth fluoride UCNPs ($M_{1-x}Ln_xF_{2+x}$ MLnF) with a CaF_2 shell. We synthesize 8 alkaline-earth host materials doped with Yb^{3+} and Tm^{3+}, with alkaline-earth (M) spanning Ca, Sr, and Ba, MgSr, CaSr, CaBa, SrBa, and CaSrBa. We explore UCNP composition, size, and lanthanide doping-dependent emission, focusing on upconversion quantum yield (UCQY) and UV emission. UCQY values of 2.46% at 250 W cm^{-2} are achieved with 14.5 nm SrLuF@CaF_2 particles, with 7.3% of total emission in the

[*] jdionne@stanford.edu, csiefe@stanford.edu.
[+]These authors contributed equally to this work.

Conflict of interest
The authors declare no conflict of interest.

UV. In 10.9 nm SrYbF:1%Tm^{3+}@CaF_2 particles, UV emission increased to 9.9% with UCQY at 1.14%. We demonstrate dye degradation under NIR illumination using SrYbF:1%Tm^{3+}@CaF_2, highlighting the efficiency of these UCNPs and their ability to trigger photoprocesses.

Keywords

alkaline earth metals; lanthanides; nanoparticles; photophysics; upconversion

Introduction

Light-driven reactions underpin processes spanning from phototherapy, where light can control drug release or trigger therapy,[1–3] to photocatalysis, where light can oxidize contaminants in water or sterilize surfaces.[4–6] As a driving force, light is noninvasive and spatially and temporally localized. Such aspects are especially important in targeted drug delivery, where localized and tailored dosage minimize side effects and maximize successful treatment.[1–2] Typically, high-energy photons such as ultraviolet (UV) or short wavelength visible light are used to trigger these systems due to the high energy barrier required to break bonds or isomerize molecules.[7–10] However, these same high energy wavelengths cannot readily penetrate biological tissues. Yb^{3+},Tm^{3+}-doped upconverting nanoparticles (UCNPs) show promise as optical converters and phototriggers for a suite of light-driven systems.[11–18] Able to absorb light in the NIR, these UCNPs can be excited deep within materials and emit light in the UV and visible through a multiphoton process, locally activating the necessary photoresponse.[11,16,17,19–25] However, in order to facilitate the use of these UCNPs, particularly towards applications that require low excitation intensity, these nanoparticles must be as bright and efficient as possible while maintaining biocompatibility.[11,15]

The efficiency of the upconversion process is strongly correlated with the nanoparticle size as well as the quality and thickness of the surface passivation provided by optically inert shell layers.[26–29] Upconversion efficiency also depends on the host lattice for the lanthanide ions, the doping concentration, and the donor-to-acceptor ratio.[30–32] The most popular host lattice for UCNPs is hexagonal-phase sodium lanthanide tetrafluoride (β-$NaLnF_4$) which is known to provide high upconversion quantum yields (UCQY) and brightness.[18,33,34] For the most common β-$NaLnF_4$ UCNPs doping ratios of 20%/0.5% for Yb^{3+}/Tm^{3+} are considered to yield efficient NIR-UV upconversion,[35,36] although the optimum doping ratio may change with the geometry (size, shell thickness, etc.) of the UCNPs and the irradiance of the excitation.[37–39] To enhance the brightness on a single particle level, the doping concentrations of the donor ion, typically Yb^{3+}, can be increased to absorb more light per nanoparticle which may result in an adjustment of the acceptor-to-donor ratio, as well.[40,41]

Recently, other new host materials have been developed that show promise for highly efficient and bright upconversion. Yang et al. demonstrated multifunctional drug delivery using $BaGdF_5$ nanoparticles doped with Yb^{3+} and Tm^{3+},[42] however, these UCNPs show little to no blue and UV emission. In other systems, upconverted light from Yb^{3+}/Tm^{3+}

doped nanoparticles have been demonstrated for drug delivery applications but still need to be further improved in terms of brightness and/or efficiency.[11,19–25,43] Strong blue upconversion emission was reported by Vetrone et al. for $BaYF_5$: Yb^{3+}, Tm^{3+}, while significant UV emission was achieved with $LiYbF_4$: Tm^{3+}, even with sub-20 nm particles.[44,45] We also demonstrated the potential of alkaline-earth rare-earth fluoride ($M_{1-x}Ln_xF_{2+x}$, MLnF) host lattices for small (sub-20 nm) lanthanide-based NIR to visible Yb^{3+}-Er^{3+} upconversion.[46] The high UCQY of these particles encouraged us to consider this new alkaline-earth host for UV and visible emission with Yb^{3+}-Tm^{3+} upconversion.

Here, we report a systematic study of the effects of alkaline-earth alloying, nanoparticle size, and Yb^{3+}-Tm^{3+} doping concentration in $M_{1-x}Ln_xF_{2+x}$ (M includes Ca^{2+}, Sr^{2+}, Ba^{2+}, and Mg^{2+}; Ln = Lu^{3+}, Yb^{3+}) nanoparticles for NIR to UV and visible upconversion. CaF_2 shells, previously shown to be biocompatible, are used for passivation to dramatically boost the upconversion efficiency of these nanoparticles by more than 5 orders of magnitude and improve their biocompatibility.[43,47–49] We synthesized 8 different core UCNPs based on different alkaline-earth combinations: 3 pure [CaLuF, SrLuF, BaLuF], 4 double-alloyed with equal ratio [(CaSr)LuF, (CaBa)LuF, (SrBa)LuF, (MgSr)LuF], and 1 triple-alloyed with equal ratio (CaSrBa)LuF. Through comparison of these alloys via upconversion quantum yield (UCQY) and decay lifetimes, we find SrLuF is the optimal host material for Yb^{3+}-Tm^{3+} upconversion with the highest efficiency of the series. We further investigate how increased doping concentration of Yb^{3+}/Tm^{3+} and larger active cores affect the upconversion emission. Comparing the branching ratios, which describe the relative proportion of emission from different states, of the Sr^{2+} host lattice, we show a shift to much greater UV emission for higher doping and larger cores. We characterize 15 nm core/shell SrLuF UCNPs with UCQY as high as 2.46±0.22% at 250 W cm^{-2}, where 7.3% of total emission is in the UV. Increasing the irradiance to 1000 W cm^{-2} enhances the fraction of UV light further to 10.3%. With higher lanthanide doping at 1000 W cm^{-2}, the proportional UV emission increases to 16.5% without compromising the high efficiency provided by the alkaline-earth host. Lastly, we demonstrate how the upconversion emission of SrYbF:1%Tm^{3+}@CaF_2 UCNPs can be leveraged for photochemistry by using NIR illumination of these UCNPs to degrade methylene blue. We show exponential decay of the main spectral feature of methylene blue via UV/Vis spectroscopy, indicating the potential for these nanoparticles as phototriggers.

Results and Discussion

The core MLnF UCNPs are colloidally synthesized via thermal decomposition of the corresponding alkaline-earth and rare-earth trifluoroacetate (CF_3COO^-, TFA) salts with a M:Ln ratio of 1:1 in oleic acid (OA), 1-octadecene (ODE), and oleylamine (OLA) at 300 °C under inert atmosphere (further details are provided in the Supporting Information, SI).[46] We use Lu^{3+} as the rare-earth component of the host materials based on previous studies that have shown higher upconversion efficiencies for MLuF UCNPs.[46,50] Efficient blue upconversion in the β-$NaLnF_4$ system is generally achieved with 20% Yb^{3+} and ≈0.5% Tm^{3+}.[51] Based on the average distance between active ions in our alkaline earth host lattices, we dope the MLnF UCNPs with 28% Yb^{3+} and 0.5% Tm^{3+} (see Supporting

Information). We synthesized 8 distinct core alkaline-earth-based UCNPs comprising M = Ca^{2+}, Sr^{2+}, and Ba^{2+} and the alloys MgSr, CaSr, CaBa, SrBa, and CaSrBa.

The 8 core MLnF UCNPs are shelled with inert CaF_2 for surface passivation. CaF_2 is not only biocompatible[43,47–49] for future in vivo applications, but also crystallizes as a face-centered cubic crystal structure with a lattice parameter (a = 5.462 Å) that is smaller than all the MLnF lattices used in this study (see SI). Therefore, the shell is grown with tensile strain, a preferred mismatch for epitaxial and isotropic shell growth.[52] The lattice mismatch increases from 1.3% to 7.8% with increasing atomic number of alkaline-earth elements of $CaYF_5$ to $BaYF_5$.

To synthesize the CaF_2 shell, a 2:3 mixture of Ca-TFA to Ca-oleate was continuously injected dropwise into the hot reaction vessel containing the washed core UCNPs at 300 °C (see SI). The injected amount of shelling precursors was adjusted to achieve nominally the same shell thickness in all samples. In a similar approach, we use TFA precursor solutions, as used for the active core synthesis, to grow larger UCNPs by injecting dropwise into the hot reaction vessel containing the washed UCNPs (see SI for further information). This process can be repeated multiple times to grow larger UCNPs. Eventually, these enlarged core UCNPs are passivated with CaF_2 shells. Figure 1 shows schematically how we can grow nanoparticle cores, followed by growing an inert or active shell or both to make larger nanoparticles. Transmission electron micrographs corresponding to these schematics are also included in Figure 1, showing core, core/inert, enlarged core, and finally enlarged core/inert shell nanoparticles. These images differentiate the CaF_2 shell and the darker MLnF core due to the higher density, and therefore stronger electron scattering, of the Lu-based host material. Images of all synthesized cores are included in the SI. Though the cores have a spherical morphology, the final sample is cubic, owing to the face-centered cubic crystal structure of both MLuF and CaF_2. The transition from spherical to cubic geometry has been discussed previously and is attributed to the smaller contribution of surface effects with increasing nanoparticle size.[46] The size of the core and the thickness of the inert shell strongly influence optical properties, such as the decay lifetimes and upconversion efficiency. To enable a fair comparison between the different alloyed nanoparticles, we synthesized particles that are as geometrically similar as possible. We define the core diameter, cube edge length, and shell thickness as shown in Figure 2 a. In general, smaller cores and thinner shells result in less efficient UCNPs. Despite their small (< 15 nm) size, the UCNPs emit very brightly when illuminated with 980 nm light (see Figure 2b). The perceived color is due to the combination of various transitions associated with Yb^{3+}-Tm^{3+} including: $^1D_2 \rightarrow {}^3F_4$ and $^1G_4 \rightarrow {}^3H_6$ in the blue and $^1G_4 \rightarrow {}^3F_4$ in the red. See SI for CIE 1976 color space map for all samples.

All samples were synthesized to be as monodisperse as possible, as is qualitatively shown with the TEM image in Figure 2 c and quantitatively plotted in the size distribution of more than 200 measurements in Figures 2d,e for the alloyed series. The standard deviation for the size of the final samples is approximately 10%. Though there exists some variability in the shell thickness, plotted in Figure 2 f, the average shell thickness of each sample is within 2–3 nm. The error of the shell thickness is propagated from the uncertainty in the core diameter and the final edge length. Differences in the size across the alloyed series may stem from

changes in the growth kinetics for these nanoparticles, potentially from different decomposition temperatures of the alkaline-earth trifluoroacetates.[46] All particles are sub-15 nm in size to ensure compatibility with a variety of applications.[53–55]

The alloyed core/shell UCNPs, dispersed in toluene, are illuminated with a 980 nm diode laser at roughly 1000 Wcm^{-2} and their emission spectra are collected using an Ocean Optics HR4000 spectrometer (see Figure 3a). A CIE 1976 color space map for all MLnF UCNCs using the spectra shown in Figure 3a is shown in the SI. Some variation in the luminescence color and relative emission intensities can be seen here, particularly in the UV. In addition, differences in the Stark level splitting are apparent, in particular in the NIR region around 780 nm. These differences are likely due to different crystal fields of host materials acting on the lanthanide ions.[36] Figure 3b depicts the relevant states of the Jablonski energy diagram for Yb^{3+}-Tm^{3+} upconversion. Here Yb^{3+} absorbs light well at 980 nm and acts as the donor for this upconversion pair, transferring energy to a nearby Tm^{3+} acceptor. Tm^{3+} can be excited multiple times yielding NIR light ($^3H_4 \rightarrow {}^3H_6$) through a two-photon process; blue ($^1G_4 \rightarrow {}^3H_6$) and red ($^1G_4 \rightarrow {}^3F_4$) light through a three-photon process; and blue ($^1D_2 \rightarrow {}^3F_4$) and UV ($^1D_2 \rightarrow {}^3H_6$) light through a four-photon process. The branching ratios, which show the proportion of emitted light in the various spectral ranges are calculated based on the integrated emission intensities of these spectra. The branching ratio for the SrLuF sample with a CaF_2 shell is plotted in Figure 3c as a function of irradiance. At higher powers the relative amount of light emitted in the red, blue, and UV increases, while that in the NIR decreases. Due to the greater number of absorbed photons required to reach these states, emission from these states is more accessible as the number of incident photons increases.[37]

Decay lifetimes can provide further insight into the photodynamics of a specific electronic transition across our alloyed series. Time-dependent luminescent measurements are shown in Figure 3d for the alloyed series. We excite the samples with a 980 nm laser pulsed at 20 Hz and detect emission at 476 nm, probing the population and depopulation of the blue ($^1G_4 \rightarrow {}^3H_6$) state of Tm^{3+}. After an initial rise time of 400–600 μs to reach maximum intensity, the upconversion emission decays exponentially. We define the decay time as the time required for the emission intensity to decrease from its maximum intensity to a factor of 1/e. All time-dependent measurements are summarized in the SI. The variation of the calculated decay times under 980 nm excitation for the emission of Yb^{3+} NIR (1000 nm), Tm^{3+} NIR (800 nm), Tm^{3+} red (650 nm), and Tm^{3+} blue (476 nm) are shown in Figure 3e. The Yb^{3+} lifetimes vary between 800–1200 μs.

Though distinct alkaline-earth host lattices do not show any apparent trend in their lifetime, we can correlate the outlier samples (CaSr)LuF, with the longest lifetime, to the thickest CaF_2 shell and BaLuF, with the shortest lifetime, to a thin CaF_2 shell (see Figure 2f). (CaSrBa)LuF has a comparably thin shell but much longer Yb^{3+} lifetime. We observed cracks in 40–60% of the CaF_2 shells on BaLuF samples, which may reduce the passivation effect and result in stronger non-radiative losses, therefore reducing the lifetime. The cracks may form because of the significant lattice mismatch between the BaLuF core and CaF_2 shell. We expect $BaLuF_5$ has similar lattice parameters than $BaYF_5$. Therefore, tensile lattice strain is around 7.8% from the core to the shell for the core/shell BaLuF sample. Such high

strain is likely too high to grow an isotropic epitaxial shell layer, explaining the imperfect CaF_2 shell for the BaLuF sample.

Upconversion quantum yield (UCQY) values are measured for the series of alkaline-earth alloyed UCNPs with CaF_2 shell dispersed in toluene at multiple irradiances of 980 nm illumination. Here we define UCQY as the number of emitted upconverted photons divided by the number of absorbed photons. Figure 4a shows the UCQY values of the total upconverted emission as well as specifically for NIR (740–860 nm), red (630–680 nm), and blue (475–530 nm) emitted light for all samples in the alloyed series measured at an irradiance of 250 Wcm^{-2}. Note that the UCQY values of the pure core MLuF samples were below the detection threshold of our measurement of 10^{-5}% and thus are not reported here. Additionally, though our samples emit in the UV, instrument limitations prevented direct quantification of the UCQY below 400 nm. However, we can estimate the contribution of the UV light on the total UCQY based on spectral measurements using an Ocean Optics spectrometer as described above with corresponding spectra shown in Figure 3a. Similarly, the reported branching ratios for upconverted NIR, red, and blue light are based on UCQY measurements while the UV branching ratio is estimated based on these spectral measurements (see SI for details). Based on this, UV emission contributes a small fraction to the overall UCQY for the alloyed samples, on average approximately 2% (see SI).

Based on the UCQY measurements, MLuF UCNPs containing Sr^{2+} are the most efficient upconverters. The core/shell SrLuF@CaF_2 is the most efficient nanoparticle sample in our series, with an UCQY value of 0.24±0.02% at 250 Wcm^{-2} and a size of 9.1±1.7 nm. We note that SrLuF was also the best performer in our previous study for Yb^{3+}/Er^{3+} upconversion.[46] Ba-based samples are also among some of the least efficient samples. We predict the cracks observed in the CaF_2 shell of the BaLuF sample are likely what reduces this sample's UCQY values, due to the reduced passivation effects as described above.

We plot the power dependent UCQY for the most efficient alloy core/shell sample, SrLuF@CaF_2, in Figure 4b (see SI for all other samples). Due to the nonlinear nature of upconversion, UCQY is heavily dependent on irradiance; similarly, different upconversion pathways vary in their dependence on irradiance due to the varying number of excitation photons required for emission from a specific state.[30,56] In an ideal case, the number of absorbed photons (n) needed to populate an energy level is proportional to the slope of the power-dependent luminescence on a log-log scale—following a power law.[30] In contrast to the brightness, the UCQY follows a power law with (n—1). Note that the value n derived from this relationship can be complicated by competing photon pathways, leading to non-integral values. The NIR emission stems from a 2-photon process therefore the value of n, derived from the slope, is ≤2. Because of a negligible UV emission from energy level $^1D_2$, we can assume that blue and red emission stem from the same initial energy level $^1G_4$ but different final energy levels, the ground and first excited state, respectively. There are 3 photons needed to populate $^1G_4$, consequently n for these transitions is ≤3 in an ideal case. The deviation of lower slopes compared to the ideal case is attributed to cross-relaxation and other loss processes. We note that UCQY is consistently greater in the blue compared to the red due to the additional 4-photon process that can facilitate blue emission ($^1D_2 \rightarrow {}^3F_4$).

To investigate the effects of size and doping concentration on the UCQY, we chose to further investigate Sr-based samples because of their high efficiency. We compared SrLuF: 28% Yb^{3+}, 0.5% Tm^{3+} (SrLuF) with a completely doped sample SrYbF: 1% Tm^{3+} (SrYbF). To generate a size-series, we took the washed core samples and grew an active layer of the same material onto the cores resulting in a larger core sample (see SI for further details). We synthesized 4 sizes of SrLuF and 3 sizes of SrYbF. Table 1 summarizes nanoparticle characteristics of size, volume, and number of acceptor and donor ions per nanoparticle for the size series. On average, the smallest SrLuF and SrYbF nanoparticles have only 149 and 323 Yb^{3+} ions per nanoparticle, respectively, as well as 3 Tm^{3+} ions each. As the nanoparticle volume increases, the number of acceptor and donor ions increases rapidly along with the measured UCQY.

The emission spectra of the cores without any passivating shell is shown in Figure 5a for SrLuF and Figure 5b for SrYbF. The spectra are corrected for different absorption of the samples by accounting for the approximate number of Yb^{3+} absorbers. The ratio of UV to blue and red emission of the SrYbF sample is 2–4 times larger than that for the SrLuF sample. While the smallest SrLuF cores of less than 5 nm are barely measurable, the strong upconversion emission even in the UV can be seen from the larger, ≈11 and ≈14 nm cores. This increase in brightness is also reflected in the UCQY measurements, where the UCQY of the starting cores are below our detection threshold but increasing the size of the core dramatically increases the UCQY. We plot the UCQY as a function of nanoparticle volume in Figure 5c. This plot both highlights the significant changes in volume in this small size regime, where diameter only increases by a few nanometers, and more meaningfully represents the number of Yb^{3+} and Tm^{3+} ions in a single nanoparticle. The UCQY increases non-linearly with the UCNP volume. Such nonlinear increases can be attributed to the decreasing surface-to-volume ratio and therefore reduced surface quenching, among other effects.

We next compare the increase in emission from passivating different sized nanoparticle cores with an inert CaF_2 shell. For both host materials, SrLuF and SrYbF, the emission intensities of all spectral peaks increase significantly, as shown in Figure 6a,b. The increase is especially noticeable in the UV. For the SrLuF samples, core@CaF_2 shows very minimal, yet still apparent, UV emission while C2@CaF_2 has significant UV emission intensity comparable to other peaks. For the higher doped samples of SrYbF, core@CaF_2 shows significant UV emission, noticeably brighter than that for core@CaF_2 of SrLuF. Therefore, a higher Yb^{3+} content or more Yb^{3+} ions in a UCNP help to populate higher energy levels for stronger UV emission. The UV emission of SrYbF becomes the strongest emission line from the increased core size, as seen by C1@CaF_2 in Figure 6b. SrLuF C2@CaF_2 and SrYbF CS1@CaF_2 both show strong UV emission with branching ratio of the total UC emission at 1000 Wcm^{-2} of up to 10.5% and 16.5%, respectively.

The UCQY values for these samples are shown as a function of irradiance in Figure 6c,d. In both cases, the UCQY cannot be measured for the smallest, sub-5 nm core nanoparticles without passivation, as these values are below the detection threshold of our UCQY measurement system. Upon increase in active core size (C1, C2, and C3 for SrLuF and C1 for SrYbF), the UCQY reaches significantly higher values which is further boosted by the

passivation with CaF_2. Table 2 provides a summary of the comparison between key SrLuF and SrYbF samples once passivated with CaF_2. For SrLuF, the CaF_2 shell increases the UCQY by a factor of approximately 24 000 to 0.24±0.02% at 250 Wcm^{-2}, assuming the core sample has an UCQY at the detection threshold of 10^{-5}%. Passivating a larger core, such as C3 with a UCQY of (2.11±0.19) × 10^{-2}% at 250 Wcm^{-2}, boosts the quantum yield by a factor of 380 to 2.46±0.22% at the same irradiance. The boost in UCQY for SrYbF from core to core@CaF_2 is even more prominent, with an increase by a factor of approximately 68 500. Passivation of C1 for SrYbF yields an increase in UCQY by 240 × to 1.14±0.10% at 250 Wcm^{-2}. A table of UCQY values from relevant literature sources is provided in the SI for comparison with the values reported here.

We expect the UCQY values of the UCNPs from the SrYbF host to be less than those of the SrLuF host due to the concentration quenching effects from increased Yb^{3+} and Tm^{3+} content. In addition, the increased number of Yb^{3+} also results in faster and generally more efficient migration of excitation energy throughout the nanocrystal, including to the surface where quenching can be more prominent due to energy transfer to molecules on or near the surface and a larger number of Yb^{3+}-O^{2-} bonds, for example.[57] Energy back transfer to Yb^{3+} and Tm^{3+}-Tm^{3+} cross-relaxation could also contribute to the diminished UCQY. Furthermore, the size of the active UCNP cores are 10.8±0.7 nm for the SrLuF sample C2 and 8.1±1.1 nm for the SrYbF sample C1. By volume the SrLuF C2 core is 2.5 times larger than the SrYbF C1 core and therefore more efficient even without passivation. This is an important factor that contributes to the absolute UCQY values as well, as shown in Figure 5c.

By comparing the integrated emission intensities of the different spectral regions, we can determine the branching ratios of SrLuF and SrYbF as a function of irradiance, as shown in Figure 6e,f. Upconversion to the NIR (740–860 nm) dominates the branching ratio for both materials. We notice that SrYbF has slightly less emission than SrLuF in the blue and red but significantly more UV emission. As we would expect, we see red, blue, and UV emission increase relative to NIR emission as irradiance increases. As more photons are absorbed, higher *n* pathways become more accessible and therefore higher energy levels become more likely to be populated, which leads to stronger emission.[37]

It is also worth mentioning that the core@CaF_2 SrYbF sample has a significantly larger UCQY than the core@CaF_2 SrLuF sample despite the fact that the active core is smaller and shell thickness is almost the same. Hence, for small NIR-to-UV UCNPs, higher doping results in significant efficiency enhancement. In addition, for imaging and photoresponse applications, such as drug-delivery through photocleavage or photoisomerization, the highly doped sample also benefits from the much stronger absorption due to the larger amount of absorber per nanoparticle. As a consequence of the stronger absorption, the brightness is significantly enhanced in the SrYbF compared to the SrLuF core@CaF_2 sample. We can estimate the SrYbF core@CaF_2 sample is 10 times brighter than the comparable SrLuF core@CaF_2 sample by considering the UCQY and the number of absorbers per nanoparticle.

As a proof-of-concept NIR-trigger photoreaction, we show how upconverted light emitted by our Yb^{3+}, Tm^{3+}-doped UCNPs can be used to degrade methylene blue in chloroform.

Upon irradiation with a 980 nm diode at approximately 1000 Wcm^{-2}, we see significant changes in the UV/Vis transmission spectrum of methylene blue in the presence of SrYbF: 1% Tm UCNPs (Figure 7a). As a control, the same concentration of methylene blue is illuminated for the same amount of time without UCNPs present. As seen in Figure 7b, no change in the transmission spectrum is seen over the course of three hours of illumination. Each of these experiments were repeated three times to ensure reproducibility. Even after 5 minutes, there is a clear change in the prominent transmission feature. Plotting the percent transmission at this spectral feature as a function of time on a log-log plot (Figure 7c) shows that the dye degrades exponentially with irradiation from the UCNPs. This demonstration shows promise for these UCNPs to trigger photochemistry, such as that required for drug delivery or photodecontamination.

Conclusion

We synthesized NIR to UV and visible alkaline-earth rare-earth fluoride ($M_{1-x}Ln_xF_{2+x}$) core upconverting nanoparticles (UCNPs) doped with Yb^{3+} and Tm^{3+} in eight distinct host materials comprising alloys of Mg^{2+}, Ca^{2+}, Sr^{2+}, and Ba^{2+} and sizes of around 5 nm in diameter. We also introduced a straightforward hot injection method to grow inert, biocompatible CaF_2 shells around the core UCNPs to a total size of around 10 nm. We characterized and compared the emission spectra, time-dependent luminescence, and upconversion quantum yield (UCQY) of each host lattice. The SrLuF host lattice showed the most promise with the highest UCQY of 0.24±0.02% at 250 Wcm^{-2}. Due to this high UCQY, we further investigated the SrLnF host by growing larger core nanoparticles with an active shell layer approach and passivating them with an additional CaF_2 shell. We also explored the effect of higher doping concentrations of Yb^{3+} and Tm^{3+}. Appreciably greater UCQY was observed in these larger SrLuF core nanoparticles; when passivated with CaF_2, measured UCQY were as high as 2.46±0.22% at 250 Wcm^{-2}, significant for such 15 nm nanoparticles. When we increase the doping concentrations of Yb^{3+} and Tm^{3+} to 99% and 1%, respectively, a substantial increase in the relative emission of UV light over samples with lower doping was observed, while maintaining a high UCQY of 1.14±0.10% at 250 Wcm^{-2}, although the SrYbF sample is only 11 nm and therefore smaller than the SrLuF. For the sub-5 nm core with CaF_2 shell, SrYbF:Tm^{3+} nanoparticle outperforms the SrLuF: Yb^{3+}, Tm^{3+} nanoparticle in efficiency by a factor of 2.9 and brightness by a factor of 10, due to the higher absorption per nanoparticle. These studies emphasize the importance of core size and Yb^{3+} dopant concentration in increasing both the relative and absolute UV emission intensity, particularly in a small size regime. To the best of our knowledge, these nanoparticles are among the most efficient Yb^{3+}-Tm^{3+} upconverters in sub-15 nm size range and show high UV intensity ratio of the overall upconversion emission.[44,51,58–64] To show the viability of these nanoparticles for photochemistry, we demonstrated the ability of SrYbF: 1% Tm UCNPs to degrade methylene blue in solution with NIR excitation.

The insights provided by our work on alkaline-earth host lattices may enable high-efficiency NIR to UV and visible photo-activation, especially when small UCNPs are required. In future studies, detailed structure-property relationship studies, especially at the single-particle level, could help elucidate the benefits of certain alloys over others. We envision the our UCNPs may be especially useful for drug delivery applications, owing to the inherent

biocompatibility of the CaF_2 shell. The particle's small size and high UCQY may also find additional applications spanning solar photocatalysis, photochemistry, bioimaging, and efficient temperature, pressure, or analyte sensing.

Supplementary Material

Refer to Web version on PubMed Central for supplementary material.

Acknowledgements

S.F., C.S., and J.A.D. acknowledge support from the Photonics at Thermodynamic limits Energy Frontier Research Center, funded by the U.S. Department of Energy, Office of Science, Office of Basic Energy Sciences, under Award No. DE-SC0019140. C.S. was supported by an Eastman Kodak fellowship, NIH Grant 5R21GM129879-02, and NIH Grant 1DP2AI15207201. D.F.S acknowledges support from the Arnold and Mabel Beckman Foundation with a Postdoctoral Fellowship in the Chemical Sciences. C.A.M. and J.A.D. acknowledge financial support from the Stanford Bio-X Interdisciplinary Initiatives Committee (IIP) and NIH Grant 5R21GM129879-02. C.A.M. was supported by the Wu Tsai Neurosciences Institute and also received support from NIH Grant 1DP2AI15207201. TEM imaging was performed at the Stanford Nano Shared Facilities (SNSF), supported by the National Science Foundation under Award ECCS-1542152.

References

[1]. Brudno Y, Mooney DJ, J. Controlled Release 2015,219, 8–17.

[2]. Blum AP, Kammeyer JK, Rush AM, Callmann CE, Hahn ME, Gianneschi NC, J. Am. Chem. Soc 2015, 137, 2140–2154. [PubMed: 25474531]

[3]. Barhoumi A, Liu Q, Kohane DS, Controlled Release J 2015, 219, 31–42.

[4]. Mamaghani AH, Haghighat F, Lee C-S, Appl. Catal. B 2020, 269, 118735.

[5]. Likodimos V, Han C, Pelaez M, Kontos AG, Liu G, Zhu D, Liao S, de la Cruz AA, O'Shea K, Dunlop PSM, Byrne JA, Dionysiou DD, Falaras P, Ind. Eng. Chem. Res 2013, 52,13957–13964.

[6]. Kuwahara Y, Yamashita H, J. Mater. Chem 2011, 21, 2407–2416.

[7]. Armitage B, Chem. Rev 1998, 98, 1171–1200. [PubMed: 11848929]

[8]. Sierocki P, Maas H, Dragut P, Richardt G, Vögtle F, De Cola L, Brouwer F(AM), Zink JI, J. Phys. Chem. B 2006, 110, 24390–24398. [PubMed: 17134192]

[9]. Kim MS, Diamond SL, Bioorg. Med. Chem. Lett 2006, 16, 4007–4010. [PubMed: 16713258]

[10]. Angelos S, Choi E, Vögtle F, De Cola L, Zink JI, J. Phys. Chem. C 2007, 111, 6589 – 6592.

[11]. Jalani G, Tam V, Vetrone F, Cerruti M, J. Am. Chem. Soc 2018, 140, 10923–10931. [PubMed: 30113851]

[12]. Idris NM, Jayakumar MKG, Bansal A, Zhang Y, Chem. Soc. Rev 2015, 44, 1449–1478. [PubMed: 24969662]

[13]. Wang W, Li Y, Kang Z, Wang F, Yu JC, Appl. Catal. B 2016, 182, 184–192.

[14]. Yang M-Q, Gao M, Hong M, Ho GW, Adv. Mater 2018, 30, 1802894.

[15]. Wang C, Cheng L, Liu Z, Biomaterials 2011, 32, 1110–1120. [PubMed: 20965564]

[16]. Shen J, Zhao L, Han G, Adv. Drug Delivery Rev 2013, 65, 744–755.

[17]. Yang D, Ma P, Hou Z, Cheng Z, Li C, Lin J, Chem. Soc. Rev 2015, 44, 1416–1448. [PubMed: 24988288]

[18]. Haase M, Schäfer H, Angew. Chem. Int. Ed 2011, 50, 5808–5829;Angew. Chem 2011, 123, 5928–5950.

[19]. Chien Y-H, Chou Y-L, Wang S-W, Hung S-T, Liau M-C, Chao Y-J, Su C-H, Yeh C-S, ACS Nano 2013, 7, 8516–8528. [PubMed: 24070408]

[20]. Zhao L, Peng J, Huang Q, Li C, Chen M, Sun Y, Lin Q, Zhu L, Li F, Adv. Funct. Mater 2014, 24, 363–371.

[21]. Yao C, Wang P, Li X, Hu X, Hou J, Wang L, Zhang F, Adv. Mater 2016, 28, 9341–9348. [PubMed: 27578301]

[22]. Yan K, Chen M, Zhou S, Wu L, RSC Adv. 2016, 6, 85293–85302.
[23]. Liu J, Bu W, Pan L, Shi J, Angew. Chem. Int. Ed 2013, 52, 4375–4379;Angew. Chem 2013,125, 4471–4475.
[24]. Fedoryshin LL, Tavares AJ, Petryayeva E, Doughan S, Krull UJ, ACS Appl. Mater. Interfaces 2014, 6, 13600–13606. [PubMed: 25090028]
[25]. Yan B, Boyer J-C, Branda NR, Zhao Y, J. Am. Chem. Soc 2011,133, 19714–19717. [PubMed: 22082025]
[26]. Hudry D, Popescu R, Busko D, Diaz-Lopez M, Abeykoon M, Bordet P, Gerthsen D, Howard IA, Richards BS, J. Mater. Chem. C 2019, 7, 1164–1172.
[27]. Wang F, Wang J, Liu X, Angew. Chem. Int. Ed 2010, 49, 7456–7460;Angew. Chem 2010, 122, 7618–7622.
[28]. Würth C, Fischer S, Grauel B, Alivisatos AP, Resch-Genger U, J. Am. Chem. Soc 2018, 140, 4922–4928. [PubMed: 29570283]
[29]. Schäfer H, Ptacek P, Zerzouf O, Haase M, Adv. Funct Mater 2008, 18, 2913–2918.
[30]. Chen G, Qiu H, Prasad PN, Chen X, Chem. Rev 2014, 114, 5161–5214. [PubMed: 24605868]
[31]. Noculak A, Podhorodecki A, Pawlik G, Banski M, Misiewicz J, Nanoscale 2015, 7, 13784–13792. [PubMed: 26219227]
[32]. Noculak A, Fhui YS, Banski M, Misiewicz J, Podhorodecki A, J. Nanopart. Res 2014, 16, 2396.
[33]. Homann C, Krukewitt L, Frenzel F, Grauel B, Würth C, Resch-Genger U, Haase M, Angew. Chem. Int. Ed 2018,57,8765–8769;Angew. Chem 2018, 130, 8901–8905.
[34]. Kaiser M, Wurth C, Kraft M, Soukka T, Resch-Genger U, Nano Res. 2019, 12, 1871–1879.
[35]. Mahalingam V, Vetrone F, Naccache R, Speghini A, Capobianco JA, Adv. Mater 2009, 21, 4025–4028.
[36]. Wang F, Liu X, Chem. Soc. Rev 2009, 38, 976–989. [PubMed: 19421576]
[37]. Fischer S, Fröhlich B, Krämer KW, Goldschmidt JC, J. Phys. Chem. C 2014, 118, 30106–30114.
[38]. Gargas DJ, Chan EM, Ostrowski AD, Aloni S, Altoe MVP, Barnard ES, Sanii B, Urban JJ, Milliron DJ, Cohen BE, Schuck PJ, Nat. Nanotechnol 2014, 9, 300–305. [PubMed: 24633523]
[39]. Wen S, Zhou J, Zheng K, Bednarkiewicz A, Liu X, Jin D, Nat. Commun 2018, 9, 1–12. [PubMed: 29317637]
[40]. Ma C, Xu X, Wang F, Zhou Z, Liu D, Zhao J, Guan M, Lang CI, Jin D, Nano Lett. 2017, 17, 2858–2864. [PubMed: 28437117]
[41]. Tian B, Fernandez-Bravo A, Najafiaghdam H, Torquato NA, Altoe MVP, Teitelboim A, Tajon CA, Tian Y, Borys NJ, Barnard ES, Anwar M, Chan EM, Schuck PJ, Cohen BE, Nat. Commun 2018, 9, 1–8. [PubMed: 29317637]
[42]. Yang D, Dai Y, Liu J, Zhou Y, Chen Y, Li C, Ma P, Lin J, Biomaterials 2014, 35, 2011–2023. [PubMed: 24314558]
[43]. Shen J, Chen G, Ohulchanskyy TY, Kesseli SJ, Buchholz S, Li Z, Prasad PN, Han G, Small 2013, 9, 3213–3217. [PubMed: 23696330]
[44]. Cheng T, Marin R, Skripka A, Vetrone F, J. Am. Chem. Soc 2018, 140, 12890–12899. [PubMed: 30215515]
[45]. Vetrone F, Mahalingam V, Capobianco JA, Chem. Mater 2009, 21, 1847–1851.
[46]. Fischer S, Mehlenbacher RD, Lay A, Siefe C, Alivisatos AP, Dionne JA, Nano Lett. 2019,19, 3878–3885. [PubMed: 31056918]
[47]. Wang Y-F, Sun L-D, Xiao J-W, Feng W, Zhou J-C, Shen J, Yan C-H, Chem. Eur. J 2012, 18, 5558–5564. [PubMed: 22488939]
[48]. Dong N-N, Pedroni M, Piccinelli F, Conti G, Sbarbati A, Ramírez-Hernández JE, Maestro LM, Iglesias-de la Cruz MC, Sanz-Rodriguez E, Juarranz A, Chen F, Vetrone F, Capobianco JA, Solé JG, Bettinelli M, Jaque D, Speghini A, ACS Nano 2011, 5, 8665–8671. [PubMed: 21957870]
[49]. Chen G, Shen J, Ohulchanskyy TY, Patel NJ, Kutikov A, Li Z, Song J, Pandey RK, Ågren H, Prasad PN, Han G, ACS Nano 2012, 6, 8280–8287. [PubMed: 22928629]
[50]. Grzyb T, Przybylska D, Inorg. Chem 2018, 57, 6410–6420. [PubMed: 29756764]
[51]. Wilhelm S, ACS Nano 2017, 11, 10644–10653. [PubMed: 29068198]

[52]. Johnson NJJ, van Veggel FCJM, ACS Nano 2014, 8, 10517–10527. [PubMed: 25289882]

[53]. Etoc F, Vicario C, Lisse D, Siaugue J-M, Piehler J, Coppey M, Dahan M, Nano Lett. 2015, 15, 3487–3494. [PubMed: 25895433]

[54]. Drees C, Raj AN, Kurre R, Busch KB, Haase M, Piehler J, Angew. Chem. Int. Ed 2016, 55, 11668–11672;Angew. Chem 2016, 128, 11840–11845.

[55]. Stylianopoulos T, Jain RK, Nanomed. Nanotechnol. Biol. Med 2015, 11, 1893–1907.

[56]. Pollnau M, Gamelin DR, Luthi SR, Güdel HU, Hehlen MP, Phys. Rev. B 2000, 61, 3337–3346.

[57]. Zhou J, Wen S, Liao J, Clarke C, Tawfik SA, Ren W, Mi C, Wang F, Jin D, Nat. Photonics 2018, 12, 154–158.

[58]. Hudry D, Busko D, Popescu R, Gerthsen D, Howard IA, Richards BS, J. Mater. Chem. C 2019, 7, 7371–7377.

[59]. Kraft M, Wurth C, Palo E, Soukka T, Resch-Genger U, Methods Appl. Fluoresc. 2019, 7, 024001. [PubMed: 30690440]

[60]. Liu H, Xu CT, Lindgren D, Xie H, Thomas D, Gundlach C, Andersson-Engels S, Nanoscale 2013, 5, 4770 – 4775. [PubMed: 23604490]

[61]. Chen G, Damasco J, Qiu H, Shao W, Ohulchanskyy TY, Valiev RR, Wu X, Han G, Wang Y, Yang C, Ågren H, Prasad PN, Nano Lett. 2015, 15, 7400–7407. [PubMed: 26487489]

[62]. Huang P, Zheng W, Zhou S, Tu D, Chen Z, Zhu H, Li R, Ma E, Huang M, Chen X, Angew. Chem. Int. Ed 2014, 53, 1252–1257;Angew. Chem 2014,126, 1276–1281.

[63]. Liu Q, Sun Y, Yang T, Feng W, Li C, Li F, J. Am. Chem. Soc 2011, 133, 17122–17125. [PubMed: 21957992]

[64]. Xu CT, Svenmarker P, Liu H, Wu X, Messing ME, Wallenberg LR, Andersson-Engels S, ACS Nano 2012, 6, 4788–4795. [PubMed: 22568960]

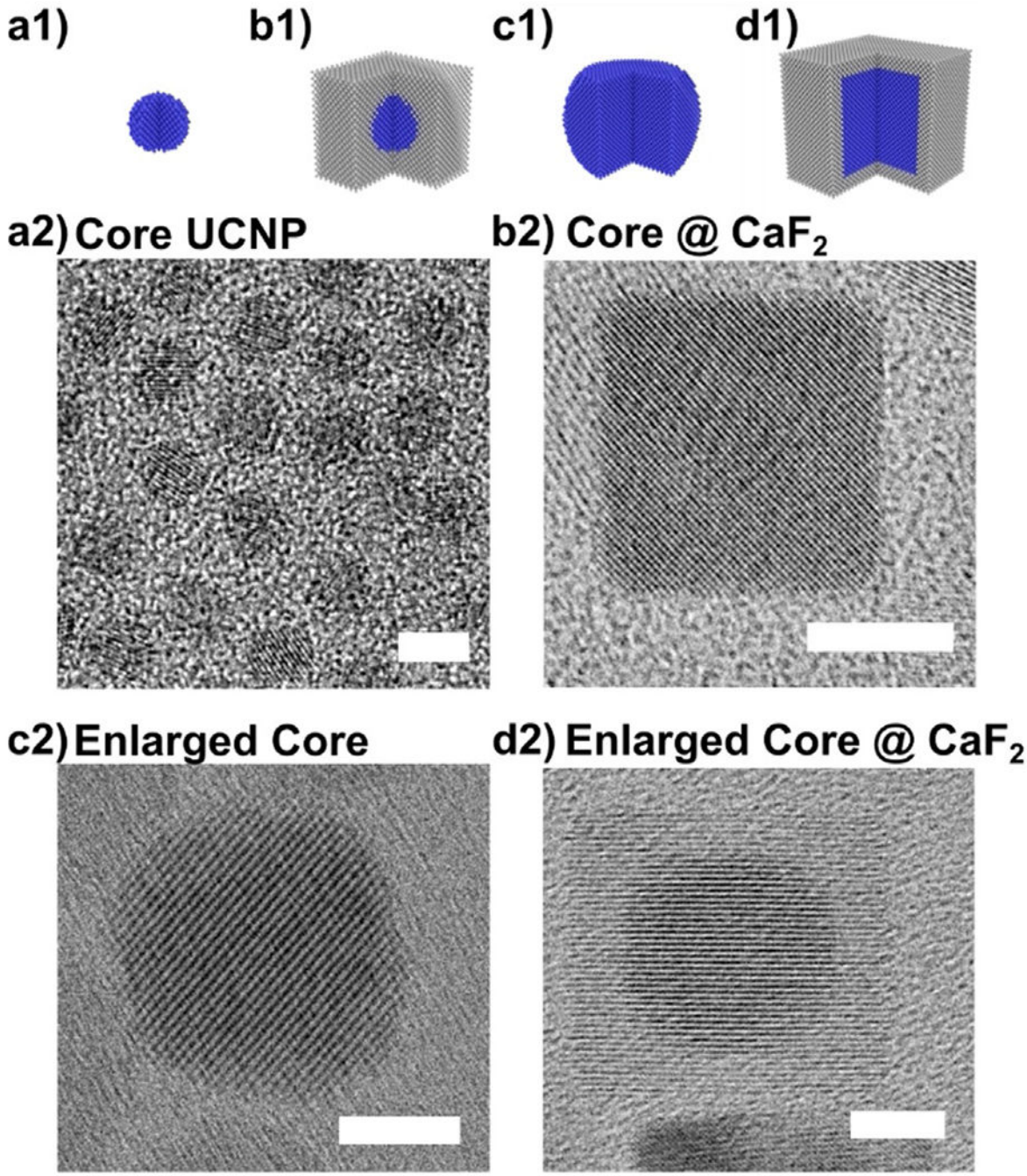

Figure 1.

Schematics and corresponding transmission electron microscope (TEM) images of a) core, b) core @ inert CaF_2 shell, c) enlarged core, and d) enlarged core @ inert CaF_2 shell nanoparticles. TEM contrast in images is due to the difference in electron scattering from the core material of heavier elements and the lighter CaF_2 shell. All scale bars are 5 nm.

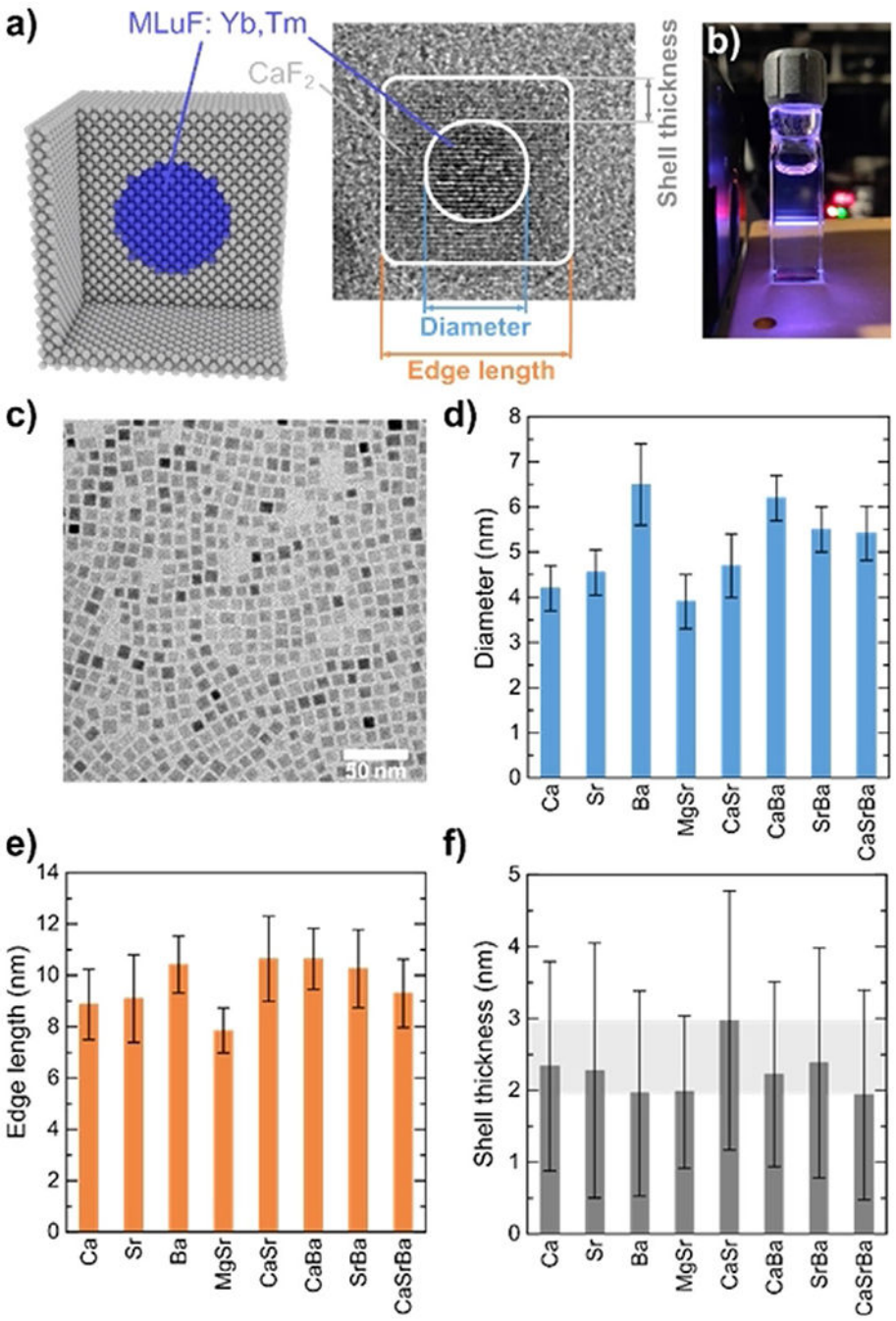

Figure 2.

a) Schematic structure of MLuF: Yb^{3+}, Tm^{3+}/CaF_2 core/shell nanoparticle and transmission electron microscope (TEM) image of single SrLuF nanoparticle for comparison. b) Picture of core/shell UCNPs dispersed in toluene and illuminated with 980 nm laser using a smartphone camera. CIE 1976 color space for all samples is shown in the Supporting Information for a quantitative color comparison at around 1000 Wcm^{-2}. c) Example TEM image of SrLuF UCNPs showing monodispersity of sample. d-f) Comparisons of core diameter, final core/shell edge length, and shell thickness, respectively, across alloyed UCNP

series. Size of the core and shell thickness strongly influence optical properties, such as the upconversion efficiency. Therefore, as similar as possible UCNP geometries were synthesized. Error bars represent the standard deviation of the measurement ($N \geq 200$). For calculation of shell thickness, error is propagated from the error associated with both the core diameter and the final edge length.

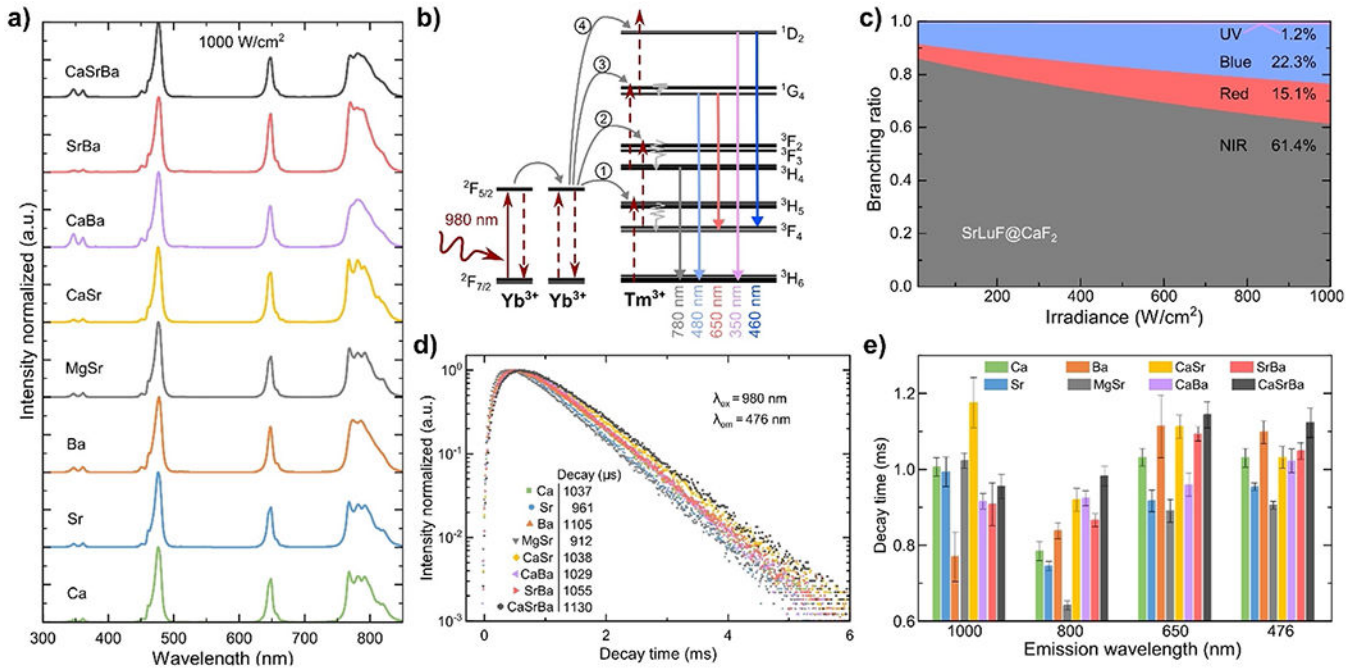

Figure 3.

a) Emission spectra of alloyed UCNP series, illuminated with a 980 nm diode laser at 1000 Wcm^{-2}, b) Schematic of the energy level diagram and the upconversion scheme. c) Branching ratio into NIR, red, blue, and UV light for $SrLuF@CaF_2$ at various illumination irradiances. d) Time-dependent upconversion measurements for alloyed series, probing the Tm^{3+} $^1G_4 \rightarrow {}^3H_6$ transition; excited at 980 nm with emission at 476 nm. e) Summary of decay lifetime measurements defined as 1/e of the peak intensity for alloyed series excited at 980 nm.

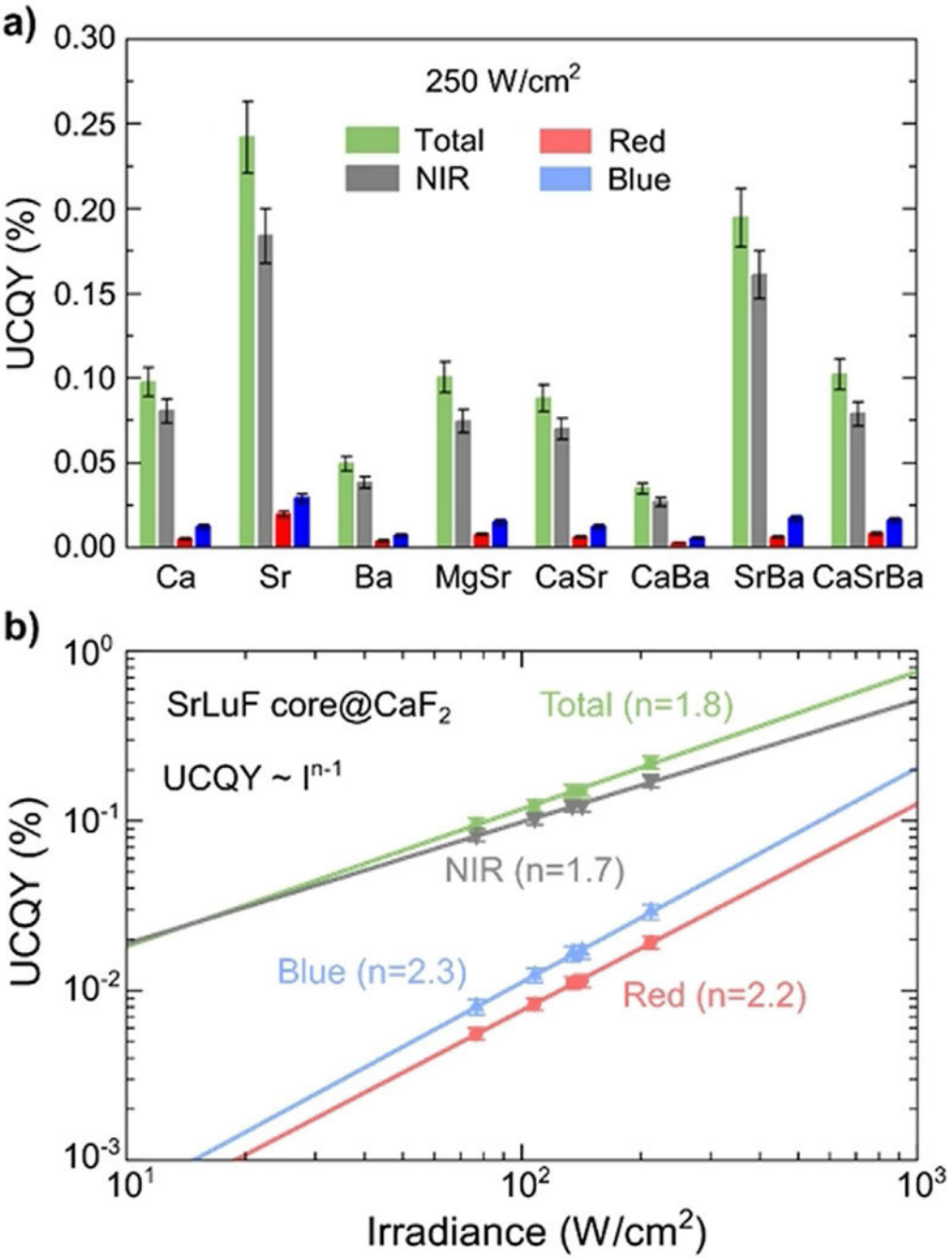

Figure 4.

a) Upconversion quantum yield (UCQY) measured for alloyed series, illuminated with a 980 nm diode laser at 250 Wcm^{-2}. b) Power-dependent example of UCQY, as a percentage, for $SrLuF@CaF_2$ on a log-log scale and fits of the power law to the data.

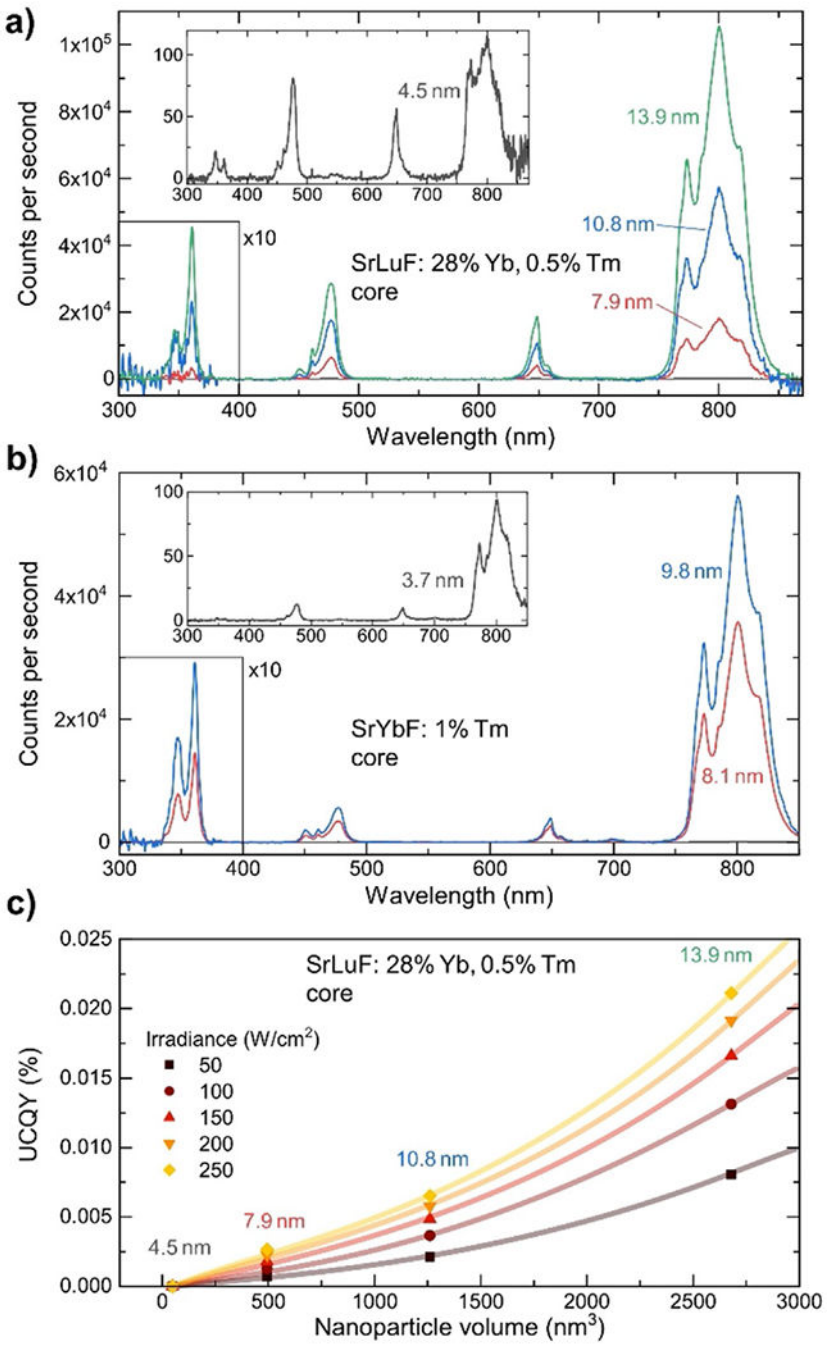

Figure 5.

Emission spectra for different core UCNP sizes without an inert shell layer for a) SrLuF: 28%Yb^{3+}, 0.5% Tm^{3+} and b) SrYbF: 1% Tm^{3+}. The region up to 400 nm is enlarged by a factor of 10. c) UCQY, as a percentage, measured at different irradiances plotted at their respective nanoparticle volumes for SrLuF: 28% Yb^{3+}, 0.5% Tm^{3+}. Increasing the UCNP size from 4.5 nm to 7.9 nm increases the volume, and therefore the number active lanthanide ions, by a factor of around 10. The UCQY increases non-linearly with UCNP volume.

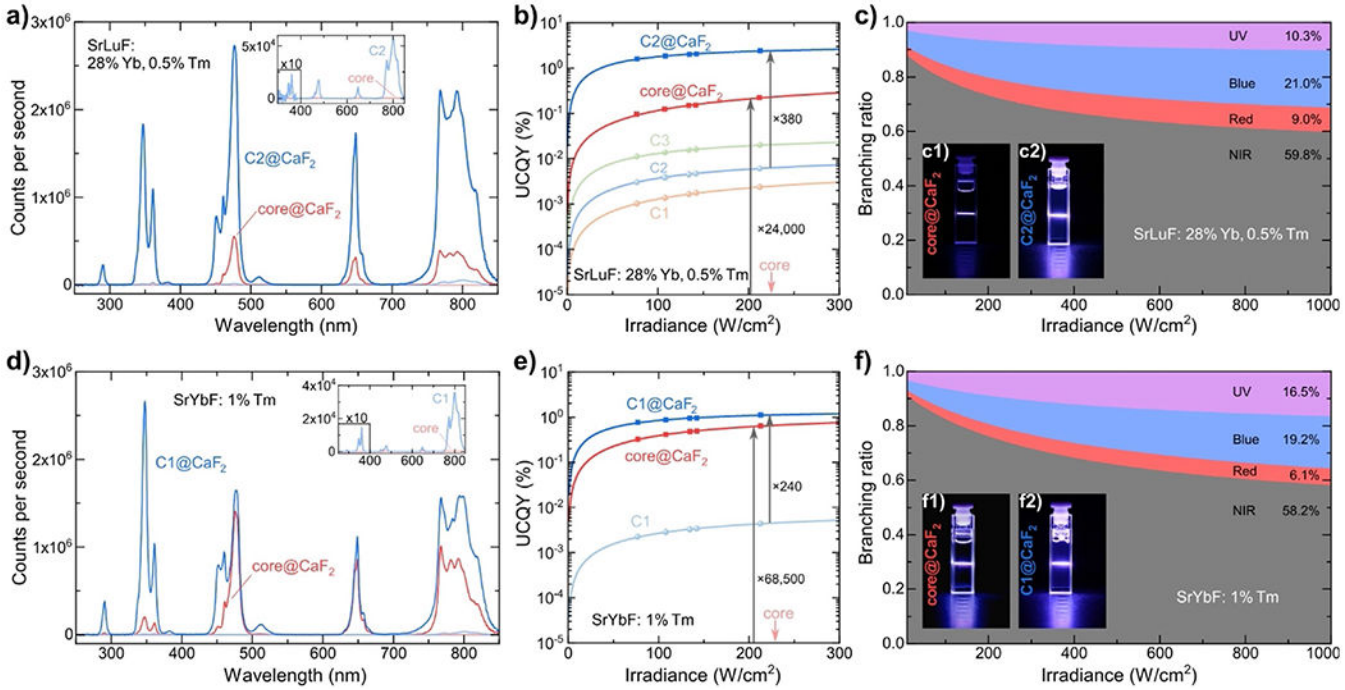

Figure 6.

Effect of nanoparticle passivation with CaF_2 shell for SrLuF: 28% Yb^{3+}, 0.5% Tm^{3+} nanoparticles on a) emission spectra, b) UCQY, as a percentage, at different irradiances, and c) branching ratios based on UCQY measurements along with digital images of the samples under 980 nm illumination. Effect of nanoparticle passivation with CaF_2 shell for SrYbF: 1% Tm^{3+} nanoparticles on d) emission spectra, e) UCQY, as a percentage, at different irradiances, and f) branching ratios based on UCQY measurements along with digital images of samples under 980 nm illumination. CIE 1976 color space maps can be found in the SI for a more quantitative discussion of luminescence color.

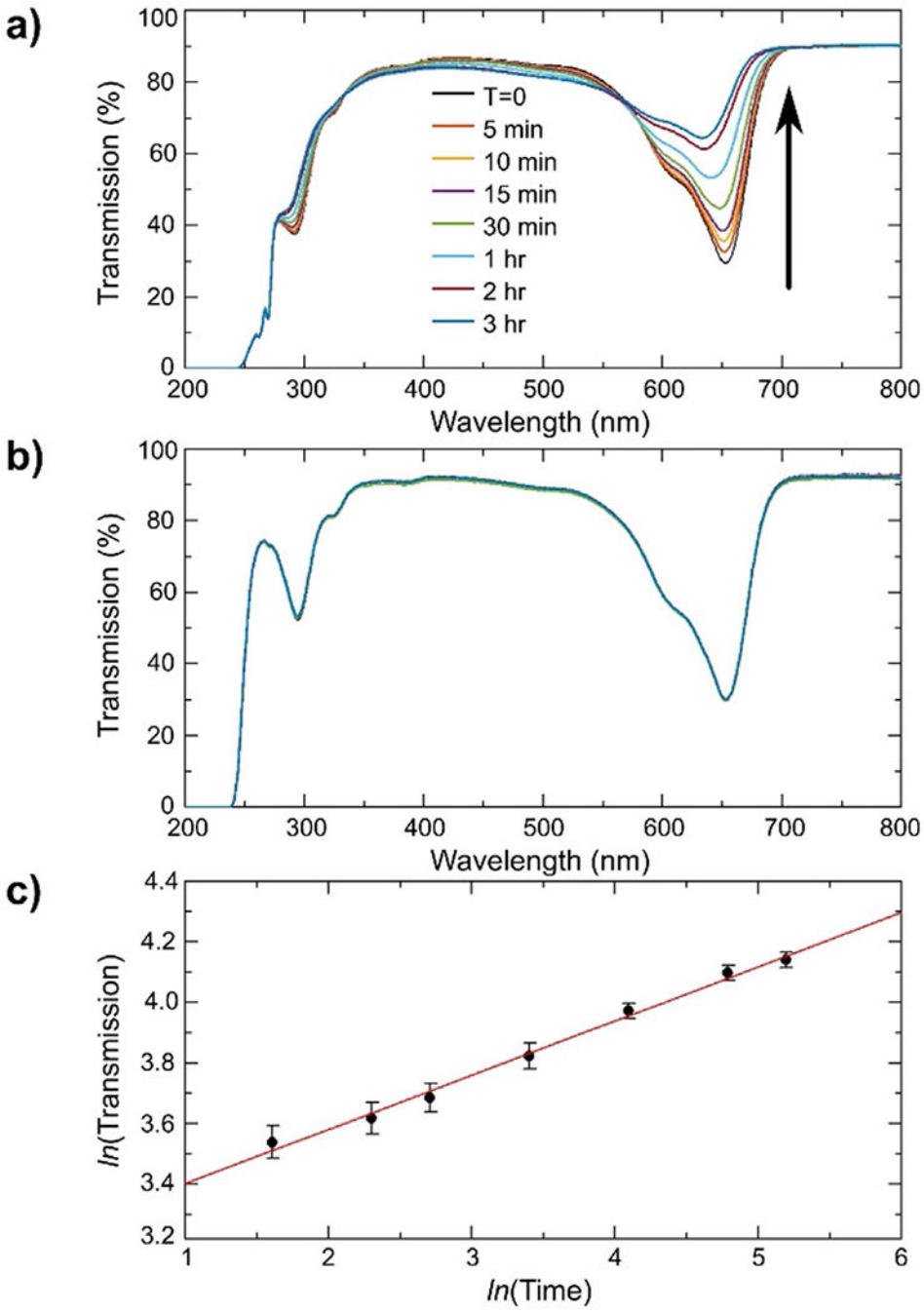

Figure 7.

UV/Vis spectra of a) UCNPs dispersed in chloroform with methylene blue dye and b) methylene blue dye dispersed in chloroform. The times corresponding to the different colored spectra refer to the illumination time of the sample with a 980 nm diode laser. c) Log–log plot of the Transmission (%) minimum over illumination time (minutes), demonstrating exponential decay. Error bars represent standard deviation of three separate

experiments. Linear fit shown in red following equation $\gamma = 0.1789*x + 3.2233$ with $R^2 = 0.9928$.

Table 1:

Summary of the core-only UCNPs and respective size, approximate volume, average number of Yb^{3+} Ions, average number of Tm^{3+} ions, and UCQY at an irradiance of 250 Wcm^{-2}. The UCQY accounts for UC emission from 400–850 nm but does not include the UV emission due to experimental limitations.

Material	Sample	Size [nm]	Volume [nm^3]	#Yb^{3+}	#Tm^{3+}	UCQY@250 [Wcm^{-2}]
SrLuF	Core	4.5±0.5	49	149	3	$< 10^{-5}$
SrLuF	C1	7.9±0.9	495	1496	27	$(0.27\pm0.02)\times10^{-2}$
SrLuF	C2	10.8±0.7	1261	3814	68	$(0.65\pm0.06)\times10^{-2}$
SrLuF	C3	13.9±1.0	2681	8106	145	$(2.11\pm0.19)\times10^{-2}$
SrYbF	Core	3.9±0.7	30	323	3	$< 10^{-5}$
SrYbF	Cl	8.1±1.1	531	5682	57	$(0.47\pm0.04)\times10^{-2}$
SrYbF	C2	9.8±1.6	928	9919	100	$(0.57\pm0.06)\times10^{-2}$

Table 2:

Summary of core/shell UCNPs including edge length of the cubic nanoparticles, the CaF_2 shell thickness, UCQY at 250 Wcm^{-2}, and proportional UV intensity. Note that the UCQY does not include the UV emission due to experimental limitations. UV intensity was determined from absorption corrected spectra to make the luminescence data comparable between the different samples. UV branching ratio was determined from the spectra shown in Figure 6a and Figure 6d at an irradiance of around 1000 Wcm^{-2}.

Material	Sample	Edge length [nm]	Shell thickness [nm]	UCQY [%][a]	UV emission intensity[b]	UV branching ratio [%][c]
SrLuF	core@CaF_2	9.1±1.7	2.3±1.8	0.24±0.02	11800	1.2
SrLuF	C2@CaF_2	14.5±1.3	1.9±1.5	2.46±0.22	207000	10.3
SrYbF	core@CaF_2	8.2±1.3	2.2±1.5	0.69±0.06	46500	3.6
SrYbF	C1@CaF_2	10.9±1.6	1.4±1.9	1.14±0.10	232000	16.5

[a] @ 250 [Wcm^{-2}].

[b] photons per second.

[c] @ 1000 [Wcm^{-2}]